mathematics

MDPI

Article

Optimal Sensor Placement Based on Fisher Information Matrix and Improved Particle Swarm Optimization Algorithm for Typical Tensile Membrane Structures

Qiu Yu [1,2,*], Xin Zhang [3], Zhiyang Jia [1,4] and Chen Peng [1,4]

[1] School of Computer Science and Technology, China University of Mining and Technology, Xuzhou 221116, China; 02232004@cumt.edu.cn (Z.J.); 02243532@cumt.edu.cn (C.P.)
[2] School of Artificial Intelligence, China University of Mining and Technology, Xuzhou 221116, China
[3] School of Information and Control Engineering, China University of Mining and Technology, Xuzhou 221116, China; zhangxin1994@cumt.edu.cn
[4] School of Mechanics and Civil Engineering, China University of Mining and Technology, Xuzhou 221116, China
* Correspondence: yuqiucumt@cumt.edu.cn

Abstract

Large-amplitude and long-term vibration deformation under external environmental loads often occurs on tensile membrane structures. Proper sensor placement plays a vital role in effectively achieving the objectives of a structural health monitoring system. In order to optimize the sensor placement to identify the modal vibration parameters for tensile membrane structures, this paper proposes an optimal sensor placement method based on the Fisher information matrix (FIM) and improved random strategy discrete particle swarm optimization algorithm (IRSDPSO). Firstly, the structural modal order is selected by using the two-norm difference and trace change rate of FIM, and the number of sensors is determined based on the QR decomposition and MAC criterion. Secondly, an improved particle swarm optimization algorithm named IRSDPSO, which has the discrete characteristic, is proposed to arrange the placement of sensors. Finally, the convergence, stability and sensitivity are used to evaluate the effectiveness of optimal sensor placement results using a numerical modal test example of the plane bidirectional tensile membrane structure. The results show that the first nineteen modal frequencies can be accurately identified. This indicates that the proposed optimal sensor placement method can determine the number of sensors and arrange the placement of the sensors. The work is reasonable and feasible in the optimal sensor placement for the tensile membrane structure.

Keywords: particle swarm optimization algorithm; optimal sensor placement; Fisher information matrix; modal assurance criterion; modal parameter identification; membrane structure

MSC: 90C59; 93E10; 62B10; 74K15

Check for updates

Academic Editors: José Carlos Ortiz-Bayliss and Ivan Mauricio Amaya-Contreras

Received: 9 May 2026
Revised: 13 June 2026
Accepted: 15 June 2026
Published: 20 June 2026

Copyright: © 2026 by the authors. Licensee MDPI, Basel, Switzerland. This article is an open access article distributed under the terms and conditions of the Creative Commons Attribution (CC BY) license.

1. Introduction

Tensile membrane structures are a new type of lightweight flexible spatial structure that emerged in the middle and late 20th century [1,2]. The long-span tensile membrane structures have damage accumulation and resistance attenuation because of external environmental loads, resulting in catastrophic accidents. According to the material characteristics and structural mechanical properties of the tensile membrane structures, the research

on the optimal sensor placement (OSP) to realize the health monitoring can effectively avoid the above problems. The problem of OSP is essentially to build an optimal number and location scheme of sensors, which can accurately obtain the dynamic response information, i.e., it can achieve the balance between the sensor cost and the system monitoring performance index [3]. The appropriate results of OSP can reduce invalid or redundant perception information, obtain the comprehensive structural response information and improve the assessment accuracy of structural health monitoring [4].

As the large complex and flexible structure, the tensile membrane structure has the characteristic of multiple degrees of freedom and complex dynamic characteristics [5]. At present, the OSP in membrane structures is mainly based on the understanding of structural vibration characteristics and empirical judgment, which is short of systematic theoretical basis and analysis. A lot of research has been carried out for the sensor placement optimization in the field of civil engineering structures over the last two decades [6,7]. Inspired by the experience of OSP in other structural detection, in order to ensure the signal-to-noise ratio of collected information and improve the efficiency of structural modal parameter identification, it is necessary to firstly establish the reasonable modeling means to determine the optimal sensor number.

The traditional OSP methods mainly rely on deterministic criteria and iterative strategies (e.g., effective independence method [8], modal assurance criterion method [9], modal kinetic energy method [10], QR decomposition method [11], singular value decomposition method [12], and Fisher information matrix method [13]), wherein the effective independent method [8] is the most classical method. Nevertheless, the MAC method [9] is very convenient for practical application because the MAC method does not need the mass matrix and stiffness matrix of structures. In addition, scholars have proposed improved methods by combining the advantages of the above methods [14–18].

As the size of the structure increases and the number of candidate measurement points increases, the OSP gradually exhibits typical discrete combination optimization characteristics. The traditional exhaustive search is almost impractical, increasing with the number of candidate measurement points. Therefore, in order to quickly obtain the effective response information that makes the identified structural modal parameters more accurate in practical application [19], some intelligent optimization technologies [20] are frequently used, i.e., sequence method (gradual accumulation method, gradual elimination method [21]), random algorithm (genetic algorithm [22–24], particle swarm optimization (PSO) algorithm [25,26], data-driven method [27], etc.). These methods are mainly based on the effective independent method and modal kinetic energy method, and usually take MAC or modal kinetic energy as the fitness function to optimize sensor locations. However, most of the existing OSP methods directly use the basic formula of the optimization algorithm to obtain suboptimal solutions, and few algorithms are improved according to the characteristics of the OSP problem model to obtain better placement effects.

The OSP has been successfully applied in conventional structures and has good performance. In order to extend OSP into tensile membrane structures to build a health monitoring system with the characteristics of high efficiency, good convenience and low cost, according to the feature of tensile membrane structures, an optimal sensor placement method based on FIM and IRSDPSO for typical tensile membrane structures is proposed in this paper. Firstly, the structural modal order of OSP is determined by using the two-norm difference and trace change rate of FIM, and the number of sensors in OSP is selected based on the QR decomposition and MAC criterion. Secondly, the optimization method, IRSDPSO, is proposed in this paper. The sensor locations are prioritized by constructing the fitness function based on the sum of mean square values of MAC off-diagonal elements. Then, the convergence, stability and sensitivity are applied to assess the effectiveness of OSP

results for tensile membrane structures. Finally, the modal parameter identification of the plane bidirectional tensile membrane structure is simulated by means of sweep excitation and transient excitation analysis in ABAQUS steady-state dynamics. This measure is to verify the proposed OSP method for the tensile membrane structure.

The main contributions are summarized as follows:

1. According to the practical engineering projects, the ABAQUS 2022 software is used to establish models of the plane bidirectional tensile membrane structure and the umbrella-shaped membrane structure respectively, which are used to optimize the OSP for the typical tensile membrane structures.
2. The selection of modal orders is based on the two-norm difference of FIM and trace change rate of FIM, and the quantity of sensors of OSP for tensile membrane structures is identified through QR decomposition and the MAC criterion.
3. The sensor location optimization of tensile membrane structure is the discrete model that the traditional PSO algorithm cannot solve. Therefore, an IRSDPSO method is proposed by improving the PSO architecture, and the fitness function is constructed based on the sum of mean square values of MAC off-diagonal elements to optimize the sensor locations for typical tensile membrane structures.

The remainder of this paper is organized as follows: The modeling processes of tensile membrane structures are briefly described in Section 2. The optimization theories of the modal order and the number of sensors in OSP for the tensile membrane structures are expounded in Section 3. The details of IRSDPSO algorithm and its fitness function are introduced in Section 4. The numerical experiments and discussion are provided in Section 5. At last, the conclusions are drawn and summarized in Section 6.

2. Modeling Analysis of Typical Tensile Membrane Structures

The membrane structure is a typical flexible structure which maintains its shape by applying pretension. Different from traditional structures, the membrane structure cannot bear bending moment, shear force or in-plane pressure. Consequently, the geometric shape state of the membrane structure depends on the extent and distribution of pretension. The plane bidirectional tensile membrane structure and the umbrella-shaped membrane structure are taken as research objects of OSP in this paper. These two membrane structures are typical of two-dimensional and three-dimensional tensile membrane structures respectively. Simulation analysis methods are widely used in numerical method analysis and validation [28]. Therefore, ABAQUS simulation software is adopted to study the natural vibration characteristics of two typical tensile membrane structures. The membrane material parameters details of the plane bidirectional tensile membrane structure and the umbrella-shaped membrane structure are set according to refs. [29] and [30] respectively. The dimension of the plane bidirectional tensile membrane structure is 1300 mm $\times$ 1300 mm square membrane as presented in Figure 1a. The boundaries of the membrane structure are free, but the four corners are set as rigid constraints, and the degrees of freedom of the corners are completely fixed accordingly. The membrane surface is meshed according to the three-node M3D3 membrane element, and the total numbers of the nodes and elements are 441 and 800 respectively. The horizontal and vertical spans of the umbrella-shaped membrane structure are 5500 mm and 700 mm separately (as shown in Figure 1b). The umbrella-shaped membrane structure adopts rigid boundaries and the degrees of freedom of the two rings up and down are also completely fixed. The membrane surface is meshed according to the four-node and three-node S4R shell element, and the total numbers of the nodes and elements are 1152 and 1126 separately.

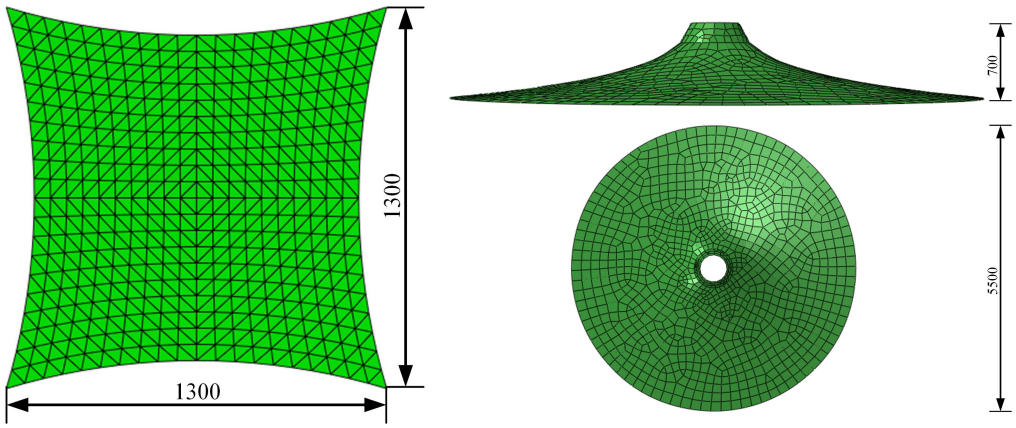


Figure 1. Geometric dimensions of typical tensile membrane structures. (**a**) The plane bidirectional tensile membrane structure. (**b**) The umbrella-shaped membrane structure.

The modeling analysis of two typical tensile membrane structures mainly includes the following three steps: Firstly, the prestress is applied to the membrane surface. Specifically, the temperature lowing method is used to apply 2.0 kN/m prestress to the plane bidirectional tensile membrane structure to achieve shape finding of the membrane structure. The small elastic modulus method is adopted to apply 3.0 kN/m prestress to the umbrella-shaped membrane structure. Secondly, the nonlinear analysis is adopted for two typical tensile membrane structures. Thirdly, the Lanzos method and mass normalization method are used to conduct modal analysis of membrane structure.

3. Quantity Optimization of OSP for Tensile Membrane Structures

3.1. Selection of Modal Orders for OSP

The two-norm has the property of measuring the closeness of adjacent modal vectors. Therefore, the contribution of each modal order vector to the modal matrix can be measured by the two-norm difference of FIM. In this paper, the mass normalized mode shapes are used to calculate FIM, and the two-norm difference and the trace change rate of FIM are used to determine the selection of modal orders. The difference between the FIM two-norms of the ith and $i+1$th modal order is used as the index to measure the impact of the target modal order. Assuming that the structure has nth modal vectors $M(1 \le i \le n-1)$, where the two-norm is $\|\Phi\|_2$. The difference between the two-norms of two neighboring modal vectors can be expressed as Equation (1). According to the norm property, it can be considered that when the difference between the two-norms of FIM is small to a certain extent, the results of two neighboring modes identification optimization are similar. In this case, only one of the modes needs to be retained as the participating mode of OSP. Analogously, we continue to compare this mode with another mode until the optimization accuracy requirements are met.

$$\mathrm{ROC}_1 = \|\Phi_{i+1}\|_2 - \|\Phi_i\|_2. \tag{1}$$

For the same reason, the number of target modes is selected by the trace change rate of FIM in combination with the eigenvalue nature of FIM as shown in Equation (2):

$$\mathrm{ROC}_2 = \frac{tr(Q_{i+1}) - tr(Q_i)}{tr(Q_i)} = \frac{tr(\Phi_{i+1}^T \Phi_{i+1}) - tr(\Phi_i^T \Phi_i)}{tr(\Phi_i^T \Phi_i)}. \tag{2}$$

The physical significance of Equations (1) and (2) is that both the two-norm difference and the trace change rate of FIM can reflect the amount of information in the matrix and

can be applied to measure the size of the matrix. The ROC value changes with the increase in the *i*th mode. When the ROC value tends to zero or changes very little, it indicates that the first i modes basically meet the requirements of mode reconstruction information of the whole structure and can obtain almost complete structural response information.

3.2. Number Selection of Sensors for OSP

When the column principal elements of the modal vector are QR decomposed, as shown in Equation (3), the norm subset with good behavior can be selected efficiently and simply. The QR decomposition method is widely adopted to select the number of sensors in OSP, as presented in Figure 2. In this paper, the successive accumulation method is used for QR decomposition, and the MAC is used as the evaluation criterion. The equation is expressed as follows:

$$\Phi^T E = QR = Q \begin{bmatrix} R_1 1 & \cdots & R_{1m} & R_{1m+1} & \cdots & R_{1n} \\ \vdots & \ddots & \vdots & \vdots & \ddots & \vdots \\ 0 & \cdots & R_{mm} & R_{mm+1} & \cdots & R_{mn} \end{bmatrix}, \tag{3}$$

where E is the permutation matrix, n is the number of degrees of freedom to be measured, M is the order of the monitored mode shape, and $Q \in R^{m\times m}$, $R \in R^{m\times n}$, $|R_{11}| > |R_{22}| > \cdots > |R_{m\times m}|$. It is noted that $E \in R^{n\times n}$ and the elements of matrix E are the positions of the structural nodes corresponding to the non-zero degree of freedoms, which are also the initial measurement points of the sensors. When R is decomposed into a combination of column vectors such as $\{r_1\}$, $\{r_1\}$, $\cdots$, $\{r_m\}$, the rows (columns) corresponding to $\{r_1\}$, $\{r_1\}$, $\cdots$, $\{r_m\}$ in $\Phi(\Phi^T)$ are the subsets of row vectors of Φ with large norm degrees of freedom.

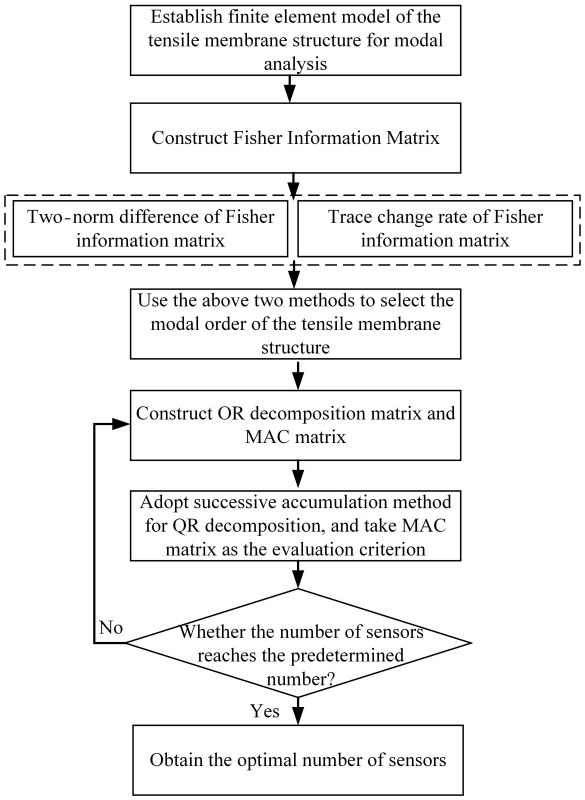


Figure 2. Selection of modal orders and number of sensors.

Assuming that $\bar{\Phi} \in R^{m\times m}$ is obtained by QR decomposition, the subset of the mode matrix composed of residual degrees of freedom of the structure is $\hat{\Phi} \in R^{(n-m)\times m}$. The

maximum off-diagonal element of $\overline{MAC}$ matrix obtained by $\bar{\Phi}$ is regarded as $\overline{MAC}_{ij}$. The $\overline{MAC}_{ij}$ is set as $(\overline{MAC}_{ij})_k$ after increasing the k-th degree of freedom of $\hat{\Phi}$:

$$\overline{MAC}_{ij} = \frac{(\bar{\Phi}_i^T \bar{\Phi}_j)^2}{(\bar{\Phi}_i^T \bar{\Phi}_i)(\bar{\Phi}_j^T \bar{\Phi}_j)} = \frac{a_{ij}^2}{a_{ii} a_{jj}}. \tag{4}$$

$$(\overline{MAC}_{ij})_k = \frac{(a_{ij} + \hat{\Phi}_{ki}\hat{\Phi}_{kj})^2}{(a_{ii} + \hat{\Phi}_{ki}^2)(a_{jj} + \hat{\Phi}_{kj}^2)} = \frac{a_{ij}^2 + [2a_{ij}\hat{\Phi}_{ki}\hat{\Phi}_{kj} + (\hat{\Phi}_{ki}\hat{\Phi}_{kj})^2]}{a_{ii}a_{jj} + [a_{ii}\hat{\Phi}_{kj}^2 + a_{jj}\hat{\Phi}_{ki}^2 + \hat{\Phi}_{ki}^2\hat{\Phi}_{kj}^2]}. \tag{5}$$

$$(\overline{MAC}_{ij})_k - \overline{MAC}_{ij} = \frac{a_{ii}a_{jj}(a_{ij} + \hat{\Phi_{ki}}\hat{\Phi_{kj}})^2 - a_{ij}^2(a_{ii} + \hat{\Phi_{ki}^2})(a_{jj} + \hat{\Phi_{kj}^2})}{a_{ii}a_{jj}(a_{ii} + \hat{\Phi_{ki}^2})(a_{jj} + \hat{\Phi_{kj}^2})}. \tag{6}$$

Equation (5) is adopted to find a degree of freedom from $\hat{\Phi}$ that can reduce $\overline{MAC}_{ij}$ to the greatest extent, and put its corresponding value in $\hat{\Phi}$. The purpose is to get the characteristic relationship curve between the maximum off-diagonal element of the MAC matrix and the number of sensors through repeating the above operations. Chang [10] proposed that the measured mode vectors are considered to be orthogonal to each other when the maximum of MAC off-diagonal elements is less than 0.25. This is usually used as a criterion for optimizing the number of sensors in OSP.

4. Sensor Location Optimization of OSP for Tensile Membrane Structures

The particle swarm optimization (PSO) algorithm is advantageous due to the few parameter settings, a straightforward structure, and excellent parallel computing ability. However, it is inappropriate to directly optimize the sensor locations by using PSO that is frequently used to solve optimization problems for continuous function models [31]. The tensile membrane structure in this paper is modeled by means of finite element mesh division, which is essentially a discrete model composed of scatter nodes. Therefore, an improved random strategy discrete improved PSO (IRSDPSO) is proposed to adapt to the sensor location optimization of OSP for tensile membrane structures in this paper. It mainly carries out the random search on the integer node domain, and each particle randomly samples the optimal node locations to retain the maximum. The optimal sensor locations are obtained by updating the particles until reaching the maximum number of iterations.

4.1. A Rounding Discrete PSO (RDPSO)

According to the characteristic of sensor location optimization for the discrete tensile membrane structure model in this paper, we carry out the rounding operation to the particle of PSO algorithm:

$$v_{id}^{t+1} = \text{round}(\omega v_{id}^t + c_1 r_1 (P_{id}^t - x_{id}^{t+1}) + c_2 r_2 (P_{gd}^t - x_{id}^{t+1})). \tag{7}$$

$$x_{id}^{t+1} = v_{id}^t + v_{id}^{t+1}. \tag{8}$$

where round$(*)$ is the rounding function, d is the particle dimension, i is the ith particle, ω is the inertia weight, and c_1 and c_2 are the self-learning factor and the social learning factor separately, which are usually positive constant. Furthermore, r_1 and r_2 are random numbers uniformly distributed on $[0, 1]$ interval to maintain the population diversity. The principle of RDPSO is the same as that of the original PSO algorithm, and the difference between these two methods is that RDPSO just adopts the rounding function to keep outputting the integer particles in the optimization search domain. This optimization method can solve simple permutation and combination problems, but more complex problems make it run slowly and be difficult to converge.

4.2. An Improved Random Strategy Discrete PSO (IRSDPSO)

4.2.1. Encoding and Decoding

In order to avoid the limitation of RDPSO in sensor location optimization, this paper uses the characteristics of the discrete tensile membrane structure model to improve the intelligent algorithm structure, and proposes an IRSDPSO. In the IRSDPSO algorithm, the variables v and x are the parallel optimization particles respectively. Assuming that there are n sensor locations for the structure with m degrees of freedom, then the dimensions of the variables v and x are $(1, 2, 3, \cdots, n)$, and the search domain of the particles is $[1, m]$. When initializing the algorithm, the IRSDPSO algorithm first randomly extracts the integer solution on the search domain between $[1, m]$ to form the initial discrete search particle positions. For the sake of avoiding repeated locations when each particle initializes and selects test points, here we set the statements for deleting repeated nodes and extract integer points again. According to the initialization particles, the local optimal solution P_{best} and the global optimal solution G_{best} of IRSDPSO algorithm are calculated using the fitness function to complete the initialization.

4.2.2. Formula Designs of Particle Velocity and Position

When traditional PSO algorithm performs optimization, the optimized models are almost elementary mathematical examples, differential equations, etc., which are continuous or partially continuous. Nonetheless, the sensor location optimization of tensile membrane structure in this paper is the discrete model, and it is impossible to solve the problem directly using the traditional PSO algorithm. For this reason, the IRSDPSO algorithm proposed in this paper modifies its particle velocity and position formulas as follows:

$$v_{in}^{t+1} = \psi_3(\psi_2(\psi_1(v_{in}^t))). \tag{9}$$

The improved velocity particle of IRSDPSO is three groups of replacement sets, where ψ_1, ψ_2 and ψ_3 represent three parts of particle velocity individually: self-velocity item, cognitive item, and social item. The last two items are determined by self-cognitive factors c_1, individual historical optimal solution P_{best}, social learning factor c_2, and global optimal solution G_{best}. The details are as follows:

$$\psi_1 = \begin{cases} \begin{cases} ev1 = \text{ceil}(d \times \text{rand}()) \\ ev2 = \text{ceil}(d \times \text{rand}()) \end{cases} & , \quad \text{rand}() < \omega \\ 0 & , \quad otherwise \end{cases}$$
$$v_{in}^{t+1} = \psi_1(v_{in}^t),\ v(i, ev1) = v(i, ev2) \tag{10}$$

$$\psi_2 = \begin{cases} \begin{cases} ep1 = \text{ceil}(d \times \text{rand}()) \\ ep2 = \text{ceil}(d \times \text{rand}()) \end{cases} & , \quad \text{rand}() < c_1 \\ 0 & , \quad otherwise \end{cases}$$
$$v_{in}^{t+1} = \psi_2(v_{in}^t),\ v(i, ep1) = P_{best}(i, ep2) \tag{11}$$

$$\psi_3 = \begin{cases} \begin{cases} eg1 = \text{ceil}(d \times \text{rand}()) \\ eg2 = \text{ceil}(d \times \text{rand}()) \end{cases} & , \quad \text{rand}() < c_2 \\ 0 & , \quad otherwise \end{cases}$$
$$v_{in}^{t+1} = \psi_3(v_{in}^t),\ v(i, eg1) = G_{best}(i, eg2) \tag{12}$$

According to the above velocity formulas of IRSDPSO, the problem of sensor location optimization for the discrete tensile membrane structure model can be well solved. The improved formulas proposed in this paper retain the simplicity of the traditional PSO

algorithm, and do not include other items except particle velocity and position. When the particle velocity formula is updated, it is helpful to retain the population diversity by randomly sampling the locations of the optimal solution during each particle search. This measure can also play a convergence role in the later stage of IRSDPSO.

4.2.3. Design of the Fitness Function

For the problem of sensor location optimization in the discrete model, this paper mainly conducts the fitness function based on the mean square values of MAC off-diagonal elements. The selected fitness function can not only consider the accuracy of parameter identification of modal tests but also ensure the effective collection of data in the process of structural health monitoring:

$$MAC_{ij} = \frac{(\phi_i^T \phi_j)^2}{(\phi_i^T \phi_i)(\phi_j^T \phi_j)}, \tag{13}$$

where $MAC_{ij}(i \neq j) \in [0, 1]$. It is noted that the smaller the MAC off-diagonal elements are, the more orthogonal and independent the mode shapes of the ith and jth mode orders are, which make it easy to distinguish them. In this paper, the goal of sensor location optimization is to minimize the sum of mean square values of MAC off-diagonal elements. The constructed fitness function f is shown below:

$$f = 1 - RMS = 1 - \sqrt{\frac{1}{n}\sum_{i=1}^{n} x_i^2}, \tag{14}$$

where RMS is the sum mean square of MAC off-diagonal elements, x_i is the MAC off-diagonal element, and n is the number of MAC off-diagonal elements. When RMS is infinitely close to 0, the fitness function f is nearly close to 1. Thereby, the problem of sensor location optimization can be transformed into the problem of solving the maximum of the fitness function f.

4.2.4. Flow Chart and Pseudocode of IRSDPSO Algorithm

The flow chart of sensor location optimization based on IRSDPSO for the discrete tensile membrane structure models is shown in Figure 3. In this paper, the particle velocity and position are updated through different judgment statements when using the IRSDPSO algorithm to optimize the sensor locations in the discrete model. The next steps are followed to optimize the sensor locations:

Step 1: Initialize the basic parameters of IRSDPSO, and set the maximum and minimum values of population number, maximum iterations, inertia weight, learning factors, and maximum and minimum values of velocity and position.

Step 2: Initialize the local optimal solution and the global optimal solution.

Step 3: Update the velocity of the particles.

Step 3.1: Replace the sensor location number in the update velocity according to the inertia weight judgment condition.

Step 3.2: Replace the sensor location number in the update velocity according to the self-cognitive factor judgment condition.

Step 3.3: Replace the sensor location number in the update velocity according to the social learning factor judgment condition.

Step 4: Compare the local optimal solution with the global optimal solution in all particles. If the local optimal solution is better than the global optimal solution, replace the sensor location number and update the sensor locations.

Step 5: Stop the operation when the maximum number of iterations reached, and output the global optimal sensor locations, otherwise go to Step 3.

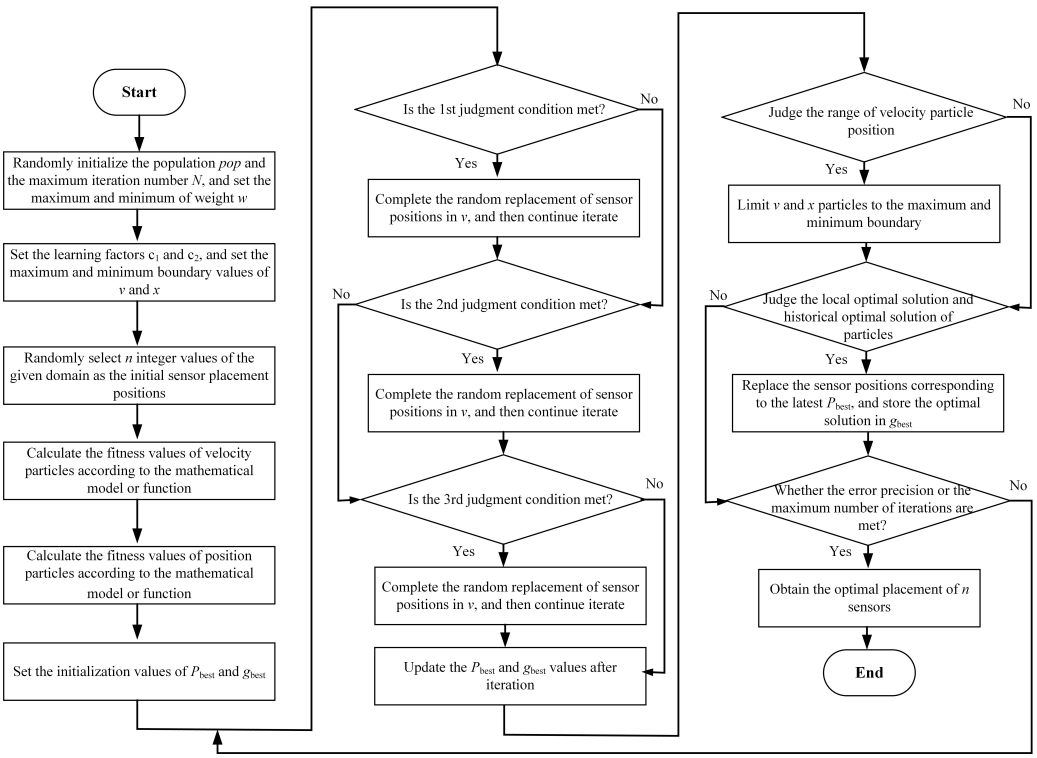


Figure 3. Flow chart of sensor location optimization based on IRSDPSO of typical tensile membrane structures.

The pseudo code of IRSDPSO proposed in this paper is shown in Algorithm 1.

Algorithm 1 Pseudo code of the IRSDPSO algorithm.

INPUT: population size pop, maximum iteration number N, dimension d, inertia weight ω, learning factors c_1, c_2
OUTPUT: velocity and position of the particle swarm
for $i = 1 : N$ **do**
  for $j = 1 : pop$ **do**
    % Velocity updating
    if $\text{rand}[0,1] < \omega$ **then**
      $v(i, \text{ceil}(d \times \text{rand}[0,1])) \leftarrow v(i, \text{ceil}(d \times \text{rand}[0,1]))$
    else if $\text{rand}[0,1] < c_1$ **then**
      $v(i, \text{ceil}(d \times \text{rand}[0,1])) \leftarrow P_{best}(i, \text{ceil}(d \times \text{rand}[0,1]))$
    else if $\text{rand}[0,1] < c_2$ **then**
      $v(i, \text{ceil}(d \times \text{rand}[0,1])) \leftarrow G_{best}(i, \text{ceil}(d \times \text{rand}[0,1]))$
    end if
    % Position updating
    if $f(v_i) < G_{best,i}$ **then**
      $x(i, \text{ceil}(d \times \text{rand}[0,1])) \leftarrow v(i, \text{ceil}(d \times \text{rand}[0,1]))$
    end if
    % The velocity and position are limited based on boundary conditions.
    % The P_{best} and G_{best} are updating according to the current swarm.
  end for
end for

5. Numerical Experiments and Discussion

5.1. Engineering Example of the Plane Bidirectional Tensile Membrane Structure

5.1.1. Importance Evaluation and Selection of the Structural Modal Order

The first eight mode shapes of the plane bidirectional tensile membrane structure are illustrated in Figure 4. When the plane bidirectional tensile membrane structure is subjected to vertical excitation, the displacement in the X and Y directions is small enough to be negligible. For this reason, only the response of Z direction is considered when optimizing OSP in this paper. It can be found from the first eight mode shapes that they are all Z direction vibration, which is also consistent with the general knowledge of the realistic vibration of the membrane structure. It is noted that the Z direction is more important than the X direction and X direction deformation, so as a simplification, only the Z direction is used to arrange single-direction sensors.

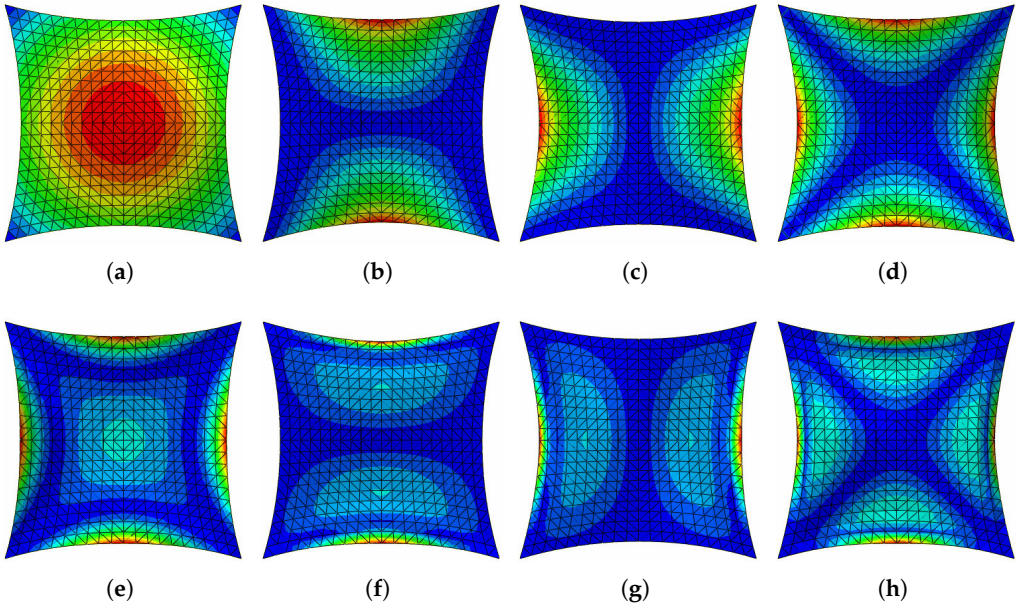


Figure 4. Mode shape diagram of the plane bidirectional tensile membrane structure. (**a**) The first mode shape. (**b**) The second mode shape. (**c**) The third mode shape. (**d**) The fourth mode shape. (**e**) The fifth mode shape. (**f**) The sixth mode shape. (**g**) The seventh mode shape. (**h**) The eighth mode shape.

Different from traditional structures, the membrane structures are characterized by low stiffness, high flexibility and other significant features. As shown in Table 1, the modal frequencies of the plane bidirectional tensile membrane structure are characterized by low-frequency, high-density and large-amplitude vibration deformation. This also explains that the membrane structures in realistic engineering applications are prone to large amplitude and long-term vibration deformation under external environmental loads.

Table 1. The first 35 modal frequencies of the plane bidirectional tensile membrane structure.

Modal order	1	2	3	4	5	6	7
Frequency/Hz	8.58	12.73	12.73	13.46	16.03	18.04	18.04
Modal order	8	9	10	11	12	13	14
Frequency/Hz	20.68	22.29	22.62	23.93	23.93	25.47	26.66
Modal order	15	16	17	18	19	20	21
Frequency/Hz	26.66	28.93	29.16	29.27	31.03	31.03	33.18
Modal order	22	23	24	25	26	27	28
Frequency/Hz	34.30	34.30	35.55	36.29	36.60	36.60	37.38
Modal order	29	30	31	32	33	34	35
Frequency/Hz	39.72	39.85	39.92	39.92	41.88	42.40	42.98

When the system generates forced vibration, high-modal orders are difficult to be excited compared with low-modal orders; thus, low-order modes often contribute the most. From the definition of modal equivalent mass, it can be seen that the greater the equivalent mass, the greater the contribution of this mode to the modal response. Generally, the equivalent mass of low-modal orders is much higher than that of high-modal orders. In short, the accumulated mass fraction can be used to roughly judge whether the number of modal orders taken is suitable. The cumulative mass fraction change curve and the importance evaluation histogram of the first one hundred modal orders of the plane bidirectional tensile membrane structure are shown in Figure 5.

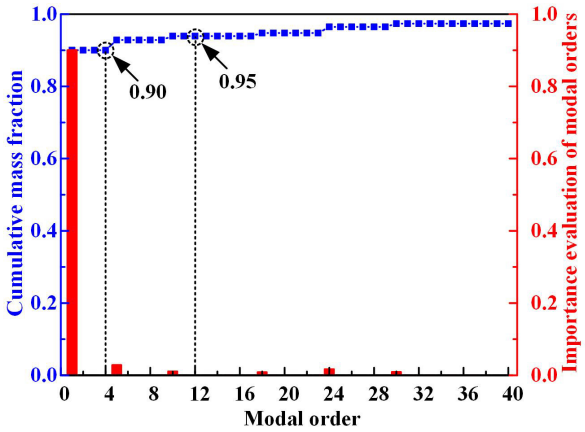


Figure 5. The values of Z-direction cumulative mass fraction of the plane bidirectional tensile membrane structure in the first one hundred modal orders.

As seen from Figure 5, it can be found that the cumulative mass fraction of the first four modal orders of the membrane structure is 0.90, and the cumulative mass fraction of the first twelve modal orders is 0.95. Based on this, it can be considered that the first twelve modal orders basically represent the overall structural information, and it can be roughly judged that the first twelve modal shapes of the plane bidirectional tensile membrane structure can meet the requirements of OSP. Furthermore, two accurate methods for selecting modal orders are applied to determine the final modal orders.

According to Equations (1) and (2), the curves of the two-norm difference and trace change rate of FIM with the first one hundred modal orders are presented in Figure 6.

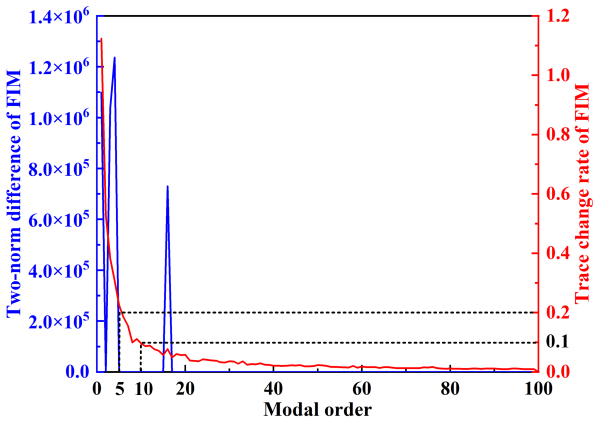


Figure 6. Curve of two-norm difference and trace change rate of FIM with number of modal orders in the plane bidirectional tensile membrane structure.

It can be seen from Figure 6 that the change of the two-norm difference value of FIM after the first five modal orders tends close to zero, which indicates that the modal

information of the first five modal orders can approximate all structural modal information. In the same way, the trace change rate of FIM shows a decreasing trend as the number of modal orders increases. When the number of modes increases from the fifth modal order to the twentieth, the decrease in trace change curve is only a minimal decrease. With the two methods above, it can be judged that the first five modal orders can meet the requirements for OSP in engineering application.

5.1.2. Number Optimization of OSP

On the basis of Equation (6), the curve of maximum of MAC off-diagonal elements changing with the number of sensors is presented in Figure 7.

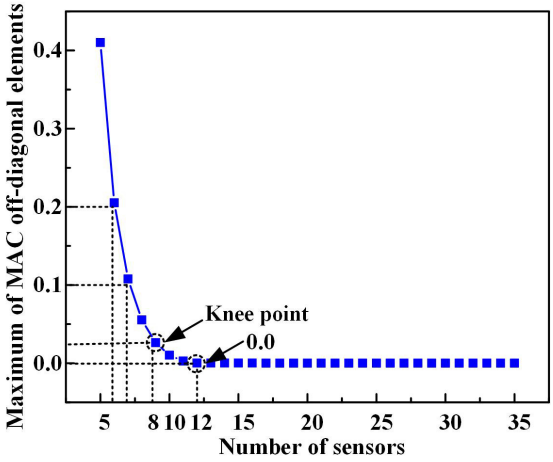


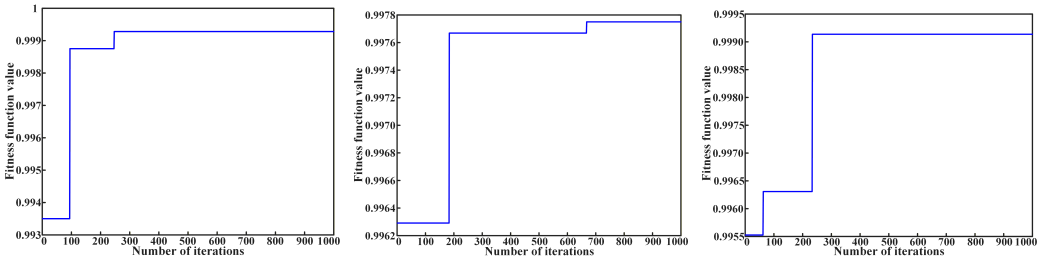
Figure 7. Curve of MAC off-diagonal element maximum value changing with the number of sensors in the plane bidirectional tensile membrane structure.

It can be seen from Figure 7 that the maximum curve of MAC off-diagonal elements has the knee point as the number of sensors increases to eight. When the number of sensors is twelve, the maximum of MAC off-diagonal elements is basically close to zero. Under these circumstances, increasing the number of sensors does not contribute much to the maximum value of MAC off-diagonal elements. In brief, if the maximum of MAC off-diagonal elements meets the requirement of less than 0.1, the optimal number of sensors would be set as eight by considering the realistic situation factors. When the number of sensors is set to twelve, the maximum of MAC off-diagonal elements is almost equal to 0, which means that the efficiency of structural modal identification is superior. In practical engineering applications, it is generally believed that the more sensors on the structure, the more information is measured. In this paper, in order to discuss the influence of different number of sensors on the OSP results, three sensor arrangement conditions (SACs) are considered. The details of the schemes are as follows: these three SACs separately select eight, ten and twelve sensor positions to be selected from all 441 nodes in the plane bidirectional tensile membrane structure. In fact, it can be observed that first SAC is the minimum number of sensors that can be used to identify the first five modal orders.

5.1.3. Results and Evaluation of Sensor Location Optimization

The two improved PSOs are used to optimize the sensor locations for the plane bidirectional tensile membrane structure. The details of basic parameters of RDPSO algorithm are as follows: The maximum and minimum of ω are set as 0.9 and 0.4 respectively, c_1 and c_2 are both set as 2, pop is 200, and the maximum of N is 1000. The iterative evolution curve of fitness function optimization based on IRSDPSO is shown in Figure 8. The particulars of the basic parameters of the IRSDPSO algorithm are as follows: ω is set as 0.6, c_1 and

c_2 are both set as 0.4, *pop* is 100, and the maximum of N is 1000. The sensor location optimization results of the plane bidirectional tensile membrane structure under the three SACs completed by RDPSO and IRSDPSO are illustrated in Table 2. The diagram of sensor distribution on the plane bidirectional tensile membrane structure is presented in Figure 9. The red dots in the figure represent the positions of sensors. The iteration time comparison between RDPSO and IRSDPSO is shown in Figure 10.

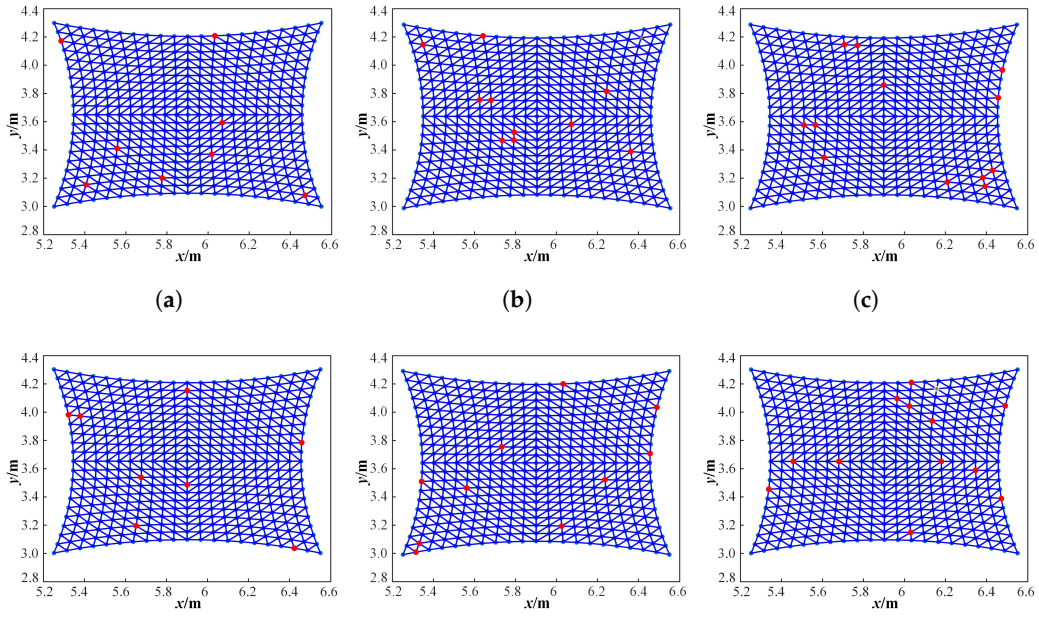


(**a**) (**b**) (**c**)

Figure 8. The iterative evolution curve of fitness function optimization based on IRSDPSO under the three SACs for the plane bidirectional tensile membrane structure. (**a**) The 1st SAC of IRSDPSO. (**b**) The 2nd SAC of IRSDPSO. (**c**) The 3rd SAC of IRSDPSO.

Table 2. Sensor location optimization results of RDPSO and IRSDPSO under different SACs for the plane bidirectional tensile membrane structure.

Method Type	The 1st SAC (8 Sensor Positions to be Selected)	The 2nd SAC (10 Sensor Positions to be Selected)	The 3rd SAC (12 Sensor Positions to be Selected)
RDPSO	161, 231, 190, 269, 124, 116, 92, 263	124, 85, 294, 209, 218, 146, 219, 343, 384, 293	185, 205, 101, 359, 239, 182, 358, 163, 104, 204, 173, 76
IRSDPSO	101, 21, 316, 265, 81, 95, 35, 211	279, 130, 188, 64, 116, 222, 100, 105, 295, 56	14, 49, 416, 42, 57, 197, 116, 424, 119, 400, 53, 105



(**a**) (**b**) (**c**)

(**d**) (**e**) (**f**)

Figure 9. Schematic diagram of sensor location optimization for the plane bidirectional tensile membrane structure. (**a**) The 1st SAC of RDPSO. (**b**) The 1st SAC of IRSDPSO. (**c**) The 2nd SAC of RDPSO. (**d**) The 2nd SAC of IRSDPSO. (**e**) The 3rd SAC of RDPSO. (**f**) The 3rd SAC of IRSDPSO.

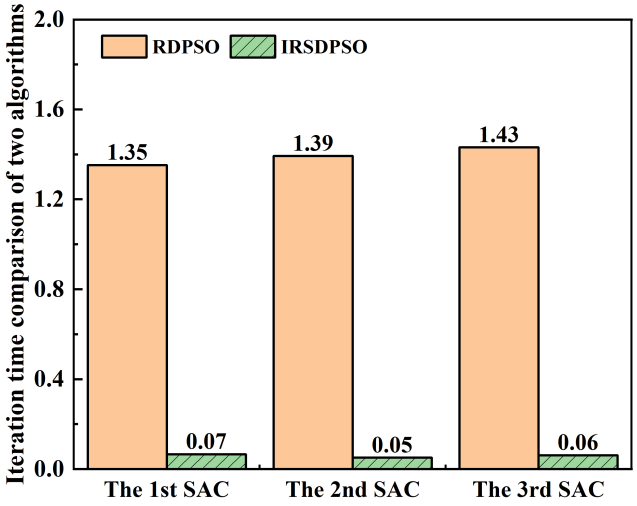


Figure 10. Iteration time comparison of RDPSO and IRSDPSO under different SACs.

It can be seen from Figure 8 that the fitness function value under different SACs based on IRSDPSO still increases step by step with the increase in the number of iterations on the basis of the initial high level. It indicates that IRSDPSO can continue searching near the initial optimal solution and find better sensor combinations. The curves tend to stabilize after about 300 iterations, and the final fitness value is close to 1, which implies that the algorithm has basically converged under the current parameter settings. The optimized sensor layout scheme has a high objective function value and good stability. Overall, the fitness function iteration curves indicate that the proposed IRSDPSO has good initial search quality, fast convergence ability, and stable optimization performance.

It can be found from Figure 9 that the sensor location result optimized by IRSDPSO is evenly distributed on the surface of the plane bidirectional tensile membrane structure by comparing with those obtained by RDPSO. There is no concentration of sensors, which avoids the information redundancy. As seen from Figure 10 the iteration time of IRSDPSO is significantly reduced compared with RDPSO, which indicates that IRSDPSO remarkably improves the efficiency of particles in spatial domain searching for the sensor arrangement locations of the tensile membrane structure, and has good capabilities of exploration and exploitation.

It is necessary to ensure that the measured modal vectors are as linearly independent of each other as possible. The degree of linear independence of the measured modal order in OSP can be evaluated by checking the value of MAC off-diagonal element. The MAC values for RDPSO and IRSDPSO under different SACs are shown in Figure 11. It can be found from Figure 11a–c that the number of maximum MAC off-diagonal elements greater than 0.25 is large, and the maximum value reaches 0.65. It can be judged that the sensor measuring locations obtained by RDPSO does not well ensure the orthogonality of the collected mode shapes. However, it can be found from Figure 11d–f that the maximum of MAC off-diagonal elements of optimization sensor locations based on IRSDPSO is 0.18, and none of these values is greater than 0.25. The optimization results of IRSDPSO meet the requirements for the measurement accuracy of the modal orthogonality of practical sensor placement. It can be found that the change amplitudes of the MAC off-diagonal elements based on IRSDPSO are significantly smaller than those of RDPSO. To put it in a nutshell, IRSDPSO has better OSP efficiency than RDPSO.

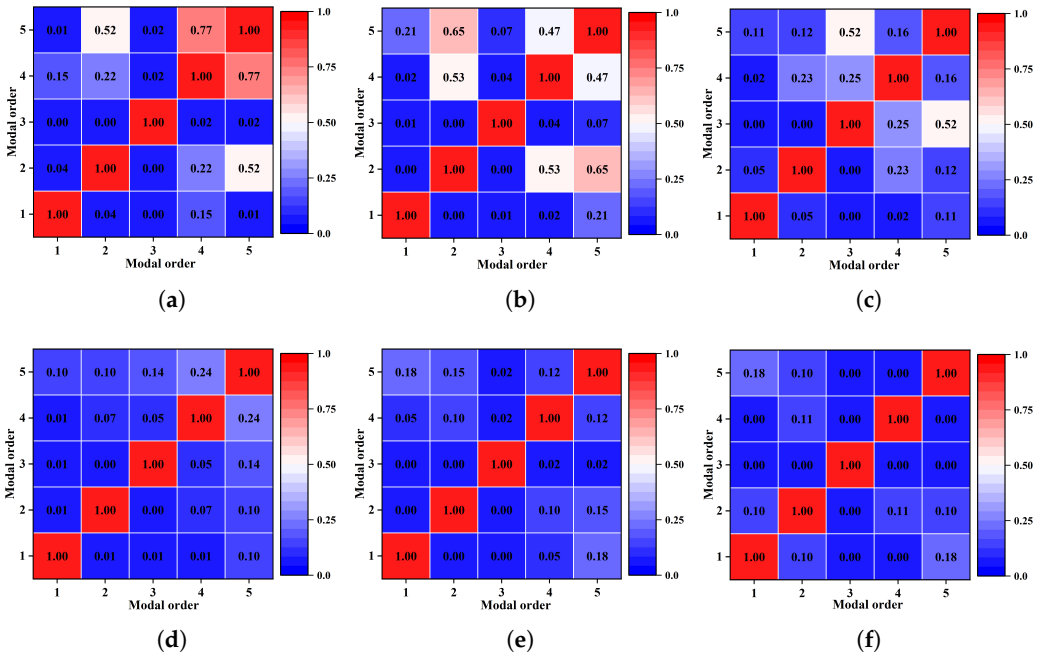


Figure 11. The MAC values for RDPSO and IRSDPSO under different SACs. (**a**) The 1st SAC of RDPSO. (**b**) The 2nd SAC of RDPSO. (**c**) The 3rd SAC of RDPSO. (**d**) The 1st SAC of IRSDPSO. (**e**) The 2nd SAC of IRSDPSO. (**f**) The 3rd SAC of IRSDPSO.

5.2. Engineering Example of the Umbrella-Shaped Membrane Structure

5.2.1. Importance Evaluation and Selection of the Structural MODAL Order

The first eight mode shapes of the umbrella-shaped membrane structure are illustrated in Figure 12. Similarly, since the Z direction is more important than the X and Y direction, as a simplification, only the Z direction is applied to arrange single direction sensors. It can be seen from Figure 12 that all Z direction vibrations have the characteristics of uniform response. The overall modal shape distribution is relatively dense, which is significantly different from that of traditional structures.

It can be seen from Table 3 that the umbrella-shaped membrane structure is characterized by light deadweight, low stiffness and high flexibility. Its natural vibration characteristics are characterized by low frequency and continuous and dense distribution. The initial prestress of the membrane surface and the structure span have a greater impact on the natural vibration frequency, and the mode shapes are more complex. This also makes this type of the membrane structure vulnerable to low-frequency, large-amplitude and long-term vibration deformation caused by external environmental loads in realistic engineering applications. These seriously endanger the structural configuration and performance.

According to Equations (1) and (2), the curves of the two-norm difference and trace change rate of FIM with first one hundred modal orders are presented in Figure 13.

It can be seen from Figure 13 that the change of the two-norm difference value of FIM after the first twelve orders tends close to zero, which indicates that the modal information of the first twelve orders can approximate whole structural modal information. For the same reason, the trace change rate of FIM shows a decreasing trend as the number of modal orders increases. When the number of modes increases from twelve to forty, the reduction of trace change curve is nearly minimal.

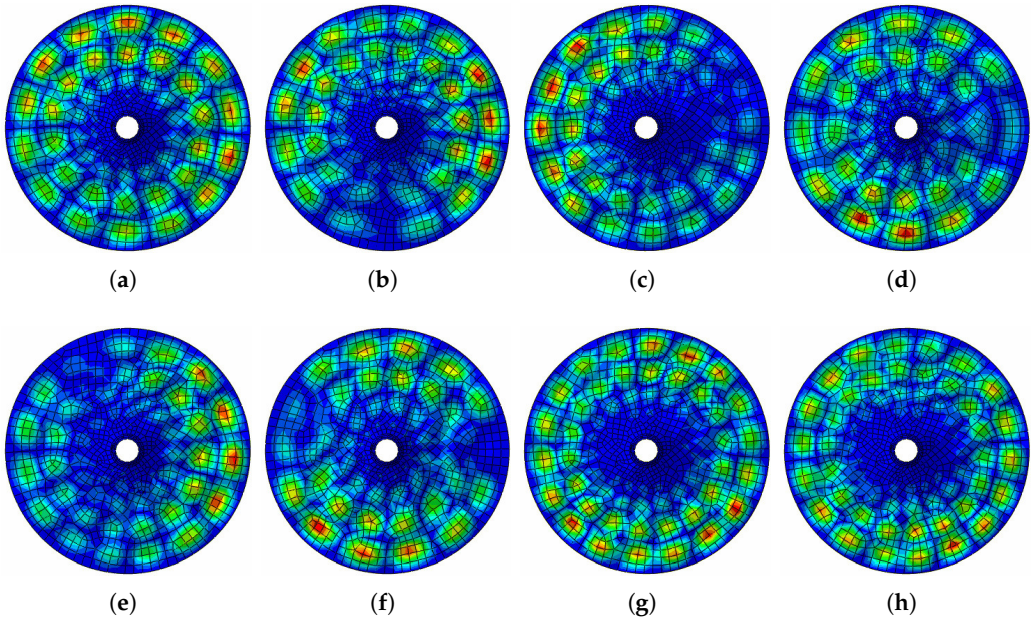


Figure 12. Mode shape diagram of the umbrella-shaped membrane structure. (**a**) The first mode shape. (**b**) The second mode shape. (**c**) The third mode shape. (**d**) The fourth mode shape. (**e**) The fifth mode shape. (**f**) The sixth mode shape. (**g**) The seventh mode shape. (**h**) The eighth mode shape.

Table 3. The first 35 modal frequencies of the umbrella-shaped membrane structure.

Modal order	1	2	3	4	5	6	7
Frequency/Hz	3.88	3.91	3.95	3.97	3.98	4.03	4.13
Modal order	8	9	10	11	12	13	14
Frequency/Hz	4.19	4.32	4.35	4.39	4.43	4.46	4.49
Modal order	15	16	17	18	19	20	21
Frequency/Hz	4.50	4.53	4.55	4.57	4.58	4.60	4.62
Modal order	22	23	24	25	26	27	28
Frequency/Hz	4.64	4.68	4.72	4.74	4.82	4.82	4.85
Modal order	29	30	31	32	33	34	35
Frequency/Hz	4.87	4.89	4.90	4.94	5.07	5.14	5.16

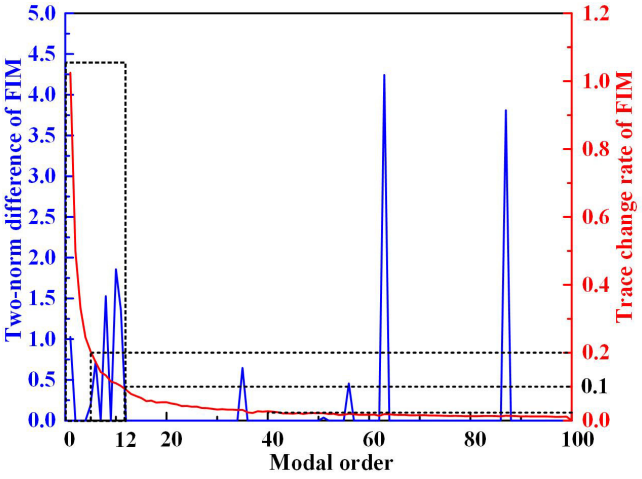


Figure 13. Curve of two-norm difference and trace change rate of FIM with number of modal orders in the umbrella-shaped membrane structure.

5.2.2. Number Optimization of OSP

On the basis of Equation (6), the curve of the maximum of MAC off-diagonal element changing with the number of sensors is presented in Figure 14.

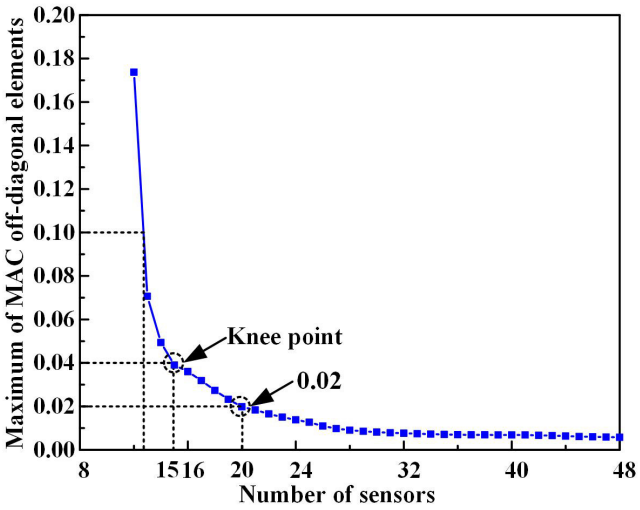
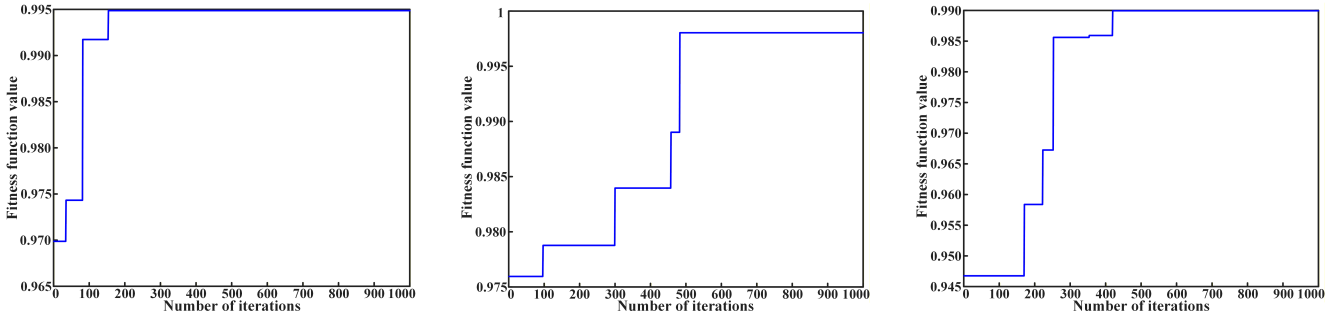


Figure 14. Curve of MAC off-diagonal element maximum value changing with the number of sensors in the umbrella-shaped membrane structure.

It can be seen from Figure 14 that the maximum of MAC off-diagonal elements decreases rapidly as the number of sensors increases to fifteen. When the number of sensors is twenty, the maximum of MAC off-diagonal element is basically close to zero. Under these circumstances, increasing the number of sensors does not contribute much to the maximum of MAC off-diagonal elements. If the maximum of MAC off-diagonal elements meets the requirement of less than 0.20, and the realistic situation factors are comprehensively considered, the optimal number of sensors would be set as eighteen. When the number of sensors is set to twenty, the maximum of MAC off-diagonal elements is almost equal to zero, which means that the efficiency of structural modal identification is superior. In the same way, for discussing the influence of different number of sensors on the OSP results, three different SACs are considered. The SACs separately select twenty, eighteen and twenty sensor positions to be selected from all 1152 nodes in the umbrella-shaped membrane structure. In fact, it can be seen from the above that first SAC is the minimum number of sensors that can be used to identify the first twelve modal orders.

5.2.3. Results and Evaluation of Sensor Location Optimization

Similarly, Equation (14) is used as the fitness function to optimize the sensor locations of the umbrella-shaped membrane structure using the above two improved PSO algorithms respectively, and the details of parameters are the same as those of the plane bidirectional tensile membrane structure. The iterative evolution curve of fitness function optimization based on IRSDPSO is shown in Figure 15. The sensor location optimization results of the umbrella-shaped membrane structure under the three SACs completed by RDPSO and IRSDPSO are shown in Table 4. The diagram of sensor distribution on the umbrella-shaped membrane structure is presented in Figure 16. The iteration time comparison between RDPSO and IRSDPSO is shown in Figure 17.

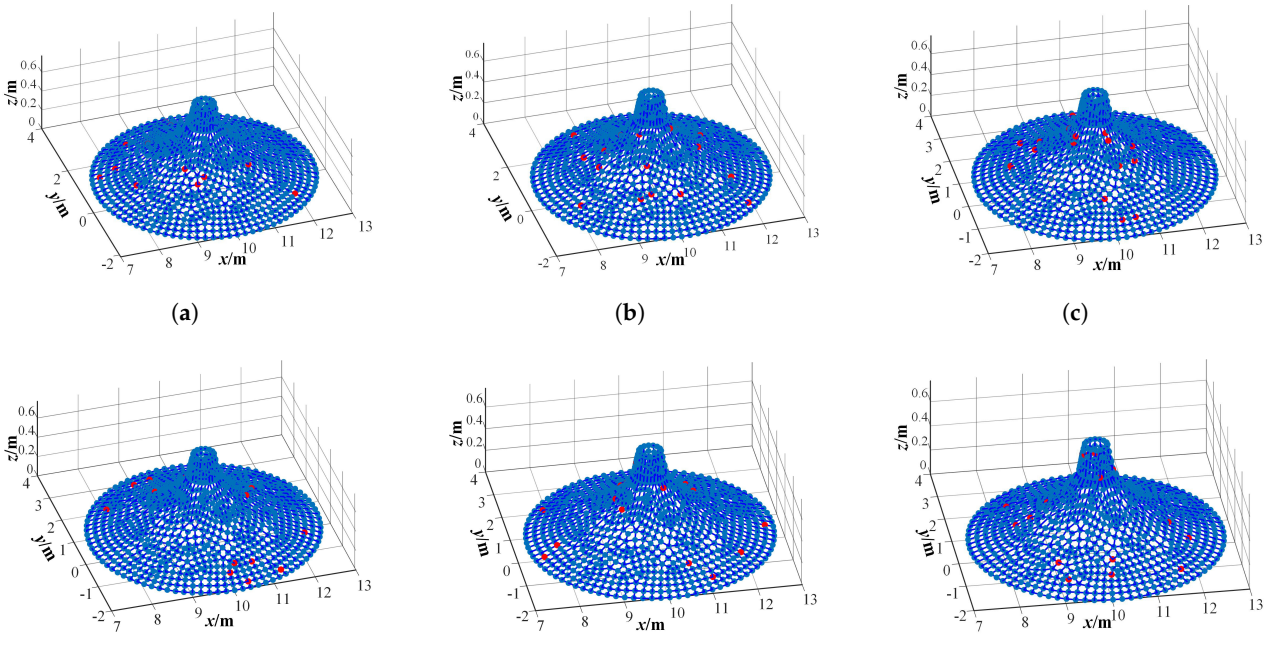


(**a**) (**b**) (**c**)

Figure 15. The iterative evolution curve of fitness function optimization based on IRSDPSO under the three SACs for the umbrella-shaped membrane structure. (**a**) The 1st SAC of IRSDPSO. (**b**) The 2nd SAC of IRSDPSO. (**c**) The 3rd SAC of IRSDPSO.

Table 4. Sensor location optimization results of RDPSO and IRSDPSO under different SACs for the umbrella-shaped membrane structure.

Method Type	The 1st SAC (15 Sensor Positions to be Selected)	The 2nd SAC (18 Sensor Positions to be Selected)	The 3rd SAC (20 Sensor Positions to be Selected)
RDPSO	537, 384, 518, 818, 655, 551, 727, 721, 314, 410, 515, 661, 578, 735, 537	550, 176, 498, 958, 934, 976, 780, 627, 669, 307, 394, 696, 742, 767, 365, 624, 593, 427	246, 509, 673, 1014, 309, 409, 589, 672, 620, 877, 494, 768, 571, 610, 506, 438, 705, 400, 706, 751
IRSDPSO	176, 361, 504, 539, 1065, 527, 280, 495, 461, 632, 234, 558, 1017, 254, 470	249, 462, 523, 490, 262, 519, 439, 836, 521, 869, 829, 954, 989, 642, 216, 334, 603, 1150	103, 496, 347, 634, 236, 97, 793, 628, 675, 797, 249, 229, 975, 502, 1138, 1080, 618, 390, 1070, 310



(**a**) (**b**) (**c**)

(**d**) (**e**) (**f**)

Figure 16. Schematic diagram of sensor location optimization for the umbrella-shaped membrane structure. (**a**) The 1st SAC of RDPSO. (**b**) The 1st SAC of IRSDPSO. (**c**) The 2nd SAC of RDPSO. (**d**) The 2nd SAC of IRSDPSO. (**e**) The 3rd SAC of RDPSO. (**f**) The 3rd SAC of IRSDPSO.

As shown in Figure 15, the proposed IRSDPSO achieves a high fitness fuction value in the initial stage, followed by a continuous step-like improvement in the first 200 iterations, and ultimately stabilizes at a level close to 1. Overall, the proposed IRSDPSO can quickly discover better sensor combinations while maintaining initial global search capability, and achieve stable convergence within a limited number of iterations. This indicates that the IRSDPSO has good initial search quality, fast convergence ability, and stable optimization performance.

It can be seen from Figure 16 that when RDPSO and IRSDPSO algorithms are used to optimize the sensor positions of the umbrella-shaped membrane structure, the sensor locations obtained from both optimization methods can be well and evenly distributed on the membrane surface. It shows that two improved discrete optimization methods have good measurement efficiency for the umbrella-shaped membrane structure. In addition, it can be seen from Figure 17 that the maximum runtime of IRSDPSO for the location optimization of umbrella membrane structure is nearly 19 times shorter than that of RDPSO. This explains that the runtime of IRSDPSO is significantly reduced compared with RDPSO, which indicates that IRSDPSO remarkable improves the efficiency of particles in spatial domain searching for the sensor arrangement locations of the tensile membrane structure, and has good exploration and exploitation capabilities.

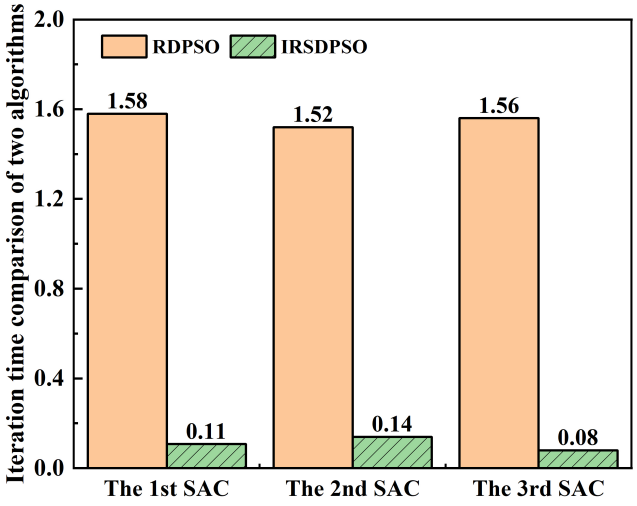


Figure 17. Histogram comparison of iteration time of RDPSO and IRSDPSO under different SACs.

The MAC values for RDPSO and IRSDPSO under different SACs are shown in Figure 16. It can be found from Figure 18a–c that the maximum number of MAC off-diagonal elements greater than 0.25 is large, and the maximum value reaches 0.64. It can be judged that the sensor measuring locations obtained by RDPSO does not well ensure the orthogonality of the collected mode shapes. However, it can be found from Figure 18d–f that the maximum number of MAC off-diagonal elements greater than 0.25 is two, and it can maintain good independent correlation of modal orders and meet the measurement accuracy requirements of actual sensor layout in general. Optimization results of IRSDPSO meet the requirements for the measurement accuracy of modal orthogonality of practical sensor placement. It can be seen that the change amplitude of the MAC off-diagonal elements based on IRSDPSO is marked lower than those of RDPSO. To put it briefly, IRSDPSO has better OSP efficiency than RDPSO.

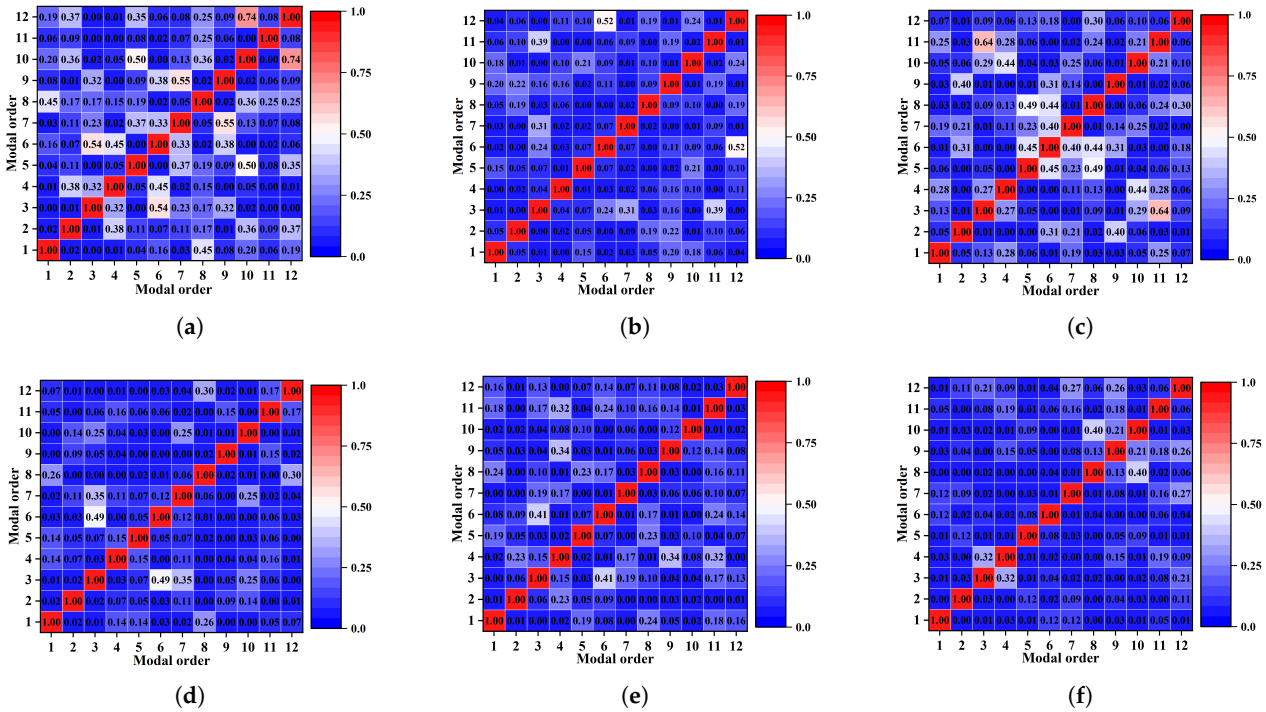


Figure 18. The MAC values for RDPSO and IRSDPSO under different SACs. (**a**) The 1st SAC of RDPSO. (**b**) The 2nd SAC of RDPSO. (**c**) The 3rd SAC of RDPSO. (**d**) The 1st SAC of IRSDPSO. (**e**) The 2nd SAC of IRSDPSO. (**f**) The 3rd SAC of IRSDPSO.

5.3. Evaluation of OSP Results for Tensile Membrane Structures

5.3.1. Evaluation Indexes

Generally speaking, the evaluation indexes of the OSP schemes are able to estimate the physical parameter characteristics, such as the orthogonality of the modal vector, sensitivity of parameter identification and noise resistance. Moreover, the relationship between the number of sensor locations and the quality of the OSP schemes should be distinguished and analyzed. In this paper, three evaluation indexes for the OSP results are selected, namely, the convergence, stability and sensitivity. The calculation formulas for these three indexes are the determinant value of FIM, the root mean square of MAC off-diagonal elements and the sum of Gramian matrix elements, where the Gramian matrix elements and formulas are expressed as

$$Gramian_{ij} = \sum_{i=1}^{n} \sum_{j=1}^{n} | \sum_{r \in m} \phi_{ir} \phi_{jr} |, \tag{15}$$

where ϕ is the mode shape, ϕ_{ir} is the rth component of the ith mode shape, $r \in m$ indicates that r is limited to all measuring points, and n is the order of the monitored modal shape. The physical significance of the three evaluation formulas is that the determinant value of FIM can measure the information quantity of modal shape. The larger the determinant value of FIM, the better the convergence of the unbiased estimation of the OSP result. The smaller the root mean square value of MAC off-diagonal elements, the larger the spatial intersection angle of the modal vector is. This also indicates that the modal vector is better distinguished, and the identification result is more stable. The sum of the Gramian matrix elements can measure whether the measuring location is at a position with large amplitude. The larger the sum of the Gramian matrix elements, the higher the signal-to-noise ratio of the measured signal, and the better the signal sensitivity.

5.3.2. Evaluation and Comparison of OSP of Typical Tensioned Membrane Structures Under Different SACs

- Evaluation of OSP results for the plane bidirectional tensile membrane structure
  In combination with the three evaluation indexes in this paper, the sum of all elements of the Gramian matrix, the root mean square of the MAC off-diagonal elements and the determinant value of FIM of the OSP schemes for the plane bidirectional tensile membrane structure under different SACs are compared. Since the sum of the Gramian matrix elements and the FIM determinant value are too large, logarithmic functions are selected for data processing in these two indexes. The specific analysis results are shown in Table 5 and Figure 19.
  It can be seen from Table 5 and Figure 19 that the determinant values of FIM based on IRSDPSO are larger than those based on RDPSO, which also shows that the IRSDPSO optimization results can better retain the structural modal shape information, and the measuring locations have better convergence. Similarly, the values of the MAC off-diagonal elements of the IRSDPSO optimization results are also smaller than those of the RDPSO optimization results. This states that the IRSDPSO optimization results have better stability of the recognition results. Finally, by comparing the sum of Gramian matrix elements of the two algorithms, it can be found that the optimization result of RDPSO is slightly higher than that of IRSDPSO, which shows that RDPSO can maintain better measurement signal sensitivity. In addition, with the increase in the number of sensors, it can be found that the determinant value of FIM and the sum of Gramian matrix elements and the overall of the OSP based on IRSDPSO show a growing trend. The root mean square of MAC off-diagonal elements also decreases gradually, which also indicates that the measured structure information of the third SAC is more complete.
- Evaluation of OSP results in the umbrella-shaped membrane structure
  Based on the same evaluation methods, the sum of Gramian matrix elements, the root mean square of the MAC off-diagonal elements and the determinant value of FIM of the OSP schemes of the umbrella-shaped membrane structure under different SACs are compared. In the same way, since the magnitude difference of FIM determinant value is too large, logarithmic function is selected here for data processing. The transformed FIM determinant values are negative after logarithmic function processing, and thirty positive integers are added to FIM determinant values to be convenient for comparing. The details of analysis results are shown in Table 6 and Figure 20.

Table 5. Evaluation of RDPSO and IRSDPSO under different SACs for the plane bidirectional tensile membrane structure.

Type of SAC	Method Type	Index 1	Index 2	Index 3
		Sum of Gramian Matrix Elements	Root Mean Square of MAC Off-Diagonal Elements	Determinant Value of FIM
The 1st	RDPSO	6.37	1.86	55.90
	IRSDPSO	6.45	0.21	61.22
The 2nd	RDPSO	6.29	1.96	56.76
	IRSDPSO	6.63	0.16	63.66
The 3rd	RDPSO	6.59	0.89	61.17
	IRSDPSO	6.59	0.12	64.74

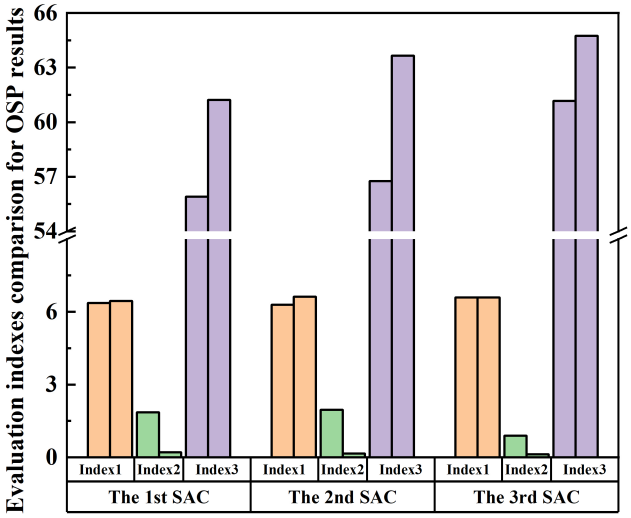


Figure 19. Comparison of evaluation indexes of RDPSO and IRSDPSO under different SACs for the plane bidirectional tensile membrane structure.

Table 6. Evaluation of RDPSO and IRSDPSO under different SACs for the umbrella-shaped membrane structure.

Type of SAC	Method Type	Index 1	Index 2	Index 3
		Sum of Gramian Matrix Elements	Root Mean Square of MAC Off-Diagonal Elements	Determinant Value of FIM
The 1st	RDPSO	36.77	7.19	3.63
	IRSDPSO	41.01	1.79	18.71
The 2nd	RDPSO	25.81	2.23	14.52
	IRSDPSO	38.02	2.11	18.52
The 3rd	RDPSO	22.84	5.43	5.88
	IRSDPSO	40.79	1.51	22.13

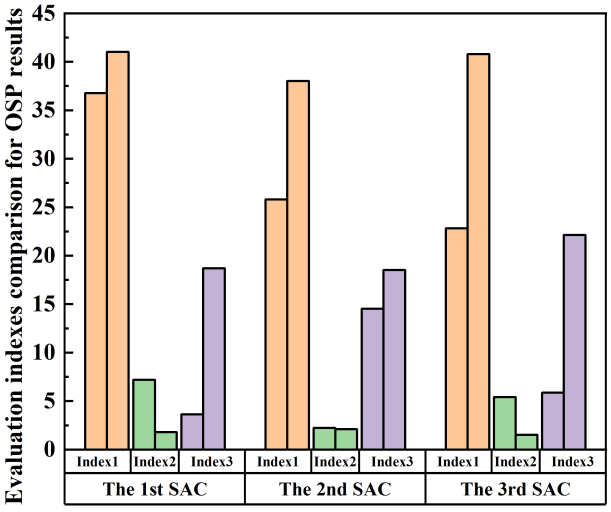


Figure 20. Comparison of evaluation indexes of RDPSO and IRSDPSO under different SACs for the umbrella-shaped membrane structure.

It can be seen from Table 6 and Figure 20 that in terms of OSP for the umbrella-shaped membrane structure, the determinant values of FIM and the sum of Gramian

matrix elements of IRSDPSO are larger than the equivalent index values of RDPSO. This indicates that the IRSDPSO optimization results can better retain the structural modal information, the convergence and the measurement signal sensitivity of sensor measuring points of corresponding OSP is better. Similarly, the values of MAC off-diagonal elements of the IRSDPSO are all smaller than those of the RDPSO, which also shows that the IRSDPSO optimization results have better stability of the modal vector identification results. In addition, with the increase in the number of sensors, the determinant values of FIM and the sum of Gramian matrix elements based on IRSDPSO show a trend of first decreasing and then increasing, while the values of MAC off-diagonal elements show a trend of first increasing and then decreasing. Although more information can be obtained by arranging enough sensors, the optimal arrangement of sensors in the umbrella-shaped membrane structure is not suitable in terms of both economy and arrangement efficiency. Therefore, it is most appropriate to choose the arrangement scheme of the first SAC in the practical measurement.

Based on the optimization and evaluation cases of different SACs, namely the plane bidirectional tensile membrane structure and the umbrella-shaped membrane structure, it can been found that the RDPSO can formally convert continuous variables into sensor candidate node numbers but does not adapt to the discrete combination characteristics of sensor position optimization from the algorithmic mechanism. The RDPSO has problems such as distorted search space mapping, unclear velocity meaning, repeated measurement points, illegal solutions, invalid iterations, premature convergence, and difficulty in handling constraints. The proposed IRSDPSO in this paper can more effectively improve global search capability, maintain population diversity, and obtain more stable and reliable sensor placement results through a search mechanism for the combination of discrete measurement points in tensile membrane structures.

5.4. Simulation and Verification of OSP Based on IRSDPSO Algorithm of the Tensile Membrane Structure

Based on the results of the above the first SAC of the OSP for the plane bidirectional tensile membrane structure, the sweep excitation and transient excitation analysis for the tensile membrane structure are carried out by using ABAQUS simulation method as shown in Figure 21. The yellow marked point pointed by the yellow arrow in Figure 21 represents the location of the excitation signal application, and the red marked point pointed by the yellow arrow represents the location of the sensor arrangement, which is used to collect the membrane surface vibration signal corresponding to the sensor arrangement position under the excitation signal. The time domain response signals are derived by taking the optimized results by IRSDPSO under the first SAC as reference locations. It is noted that the sweep excitation and transient excitation analysis are idealized validations, which does not specifically take the noise environment into consideration. The purpose of the noise-free numerical validation is not to simulate all errors in real testing but to first verify whether the proposed methodological chain itself is valid. The covariance stochastic subspace identification method based on the time-domain identification is used to identify the modal parameters of the plane bidirectional tensile membrane structure. The feasibility of the OSP based on the IRSDPSO algorithm and the effectiveness of the modal identification are verified.

The curves of sweep excitation signal and transient excitation signal of the plane bidirectional tensile membrane structure by using ABAQUS software is shown in Figure 22. The time–amplitude curves of sensor measuring locations of the plane bidirectional tensile membrane structure after excitation are presented in Figure 23. The power spectrum signal curve of the signal collected by the sensor measuring location and the modal parameter

identification of the plane bidirectional tensile membrane structure by using the covariance random machine subspace method to determine the structural natural frequency and modal order curve are shown in Figure 24 and Figure 25 respectively.

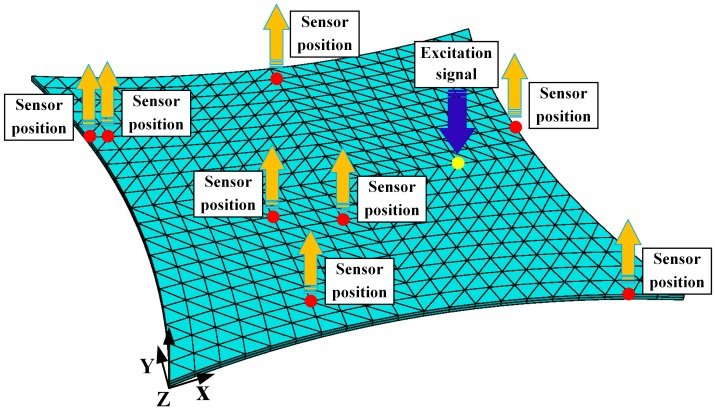


Figure 21. Simulation schematic diagram of modal test for the plane bidirectional tensile membrane structure.

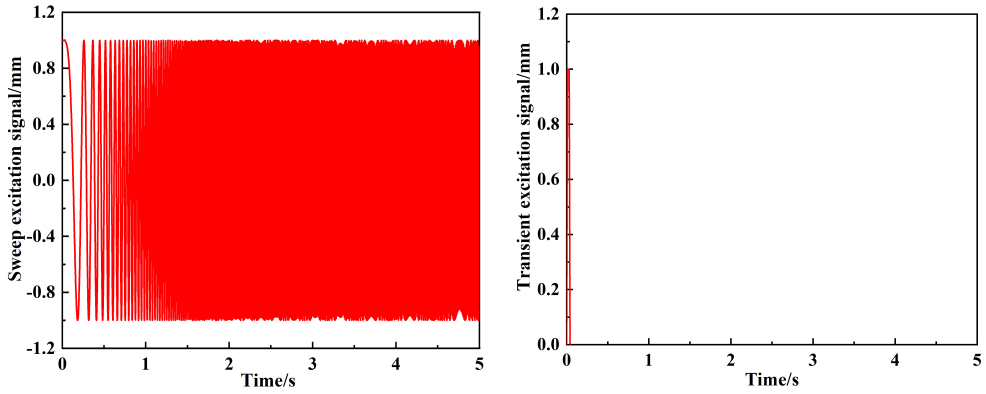


Figure 22. Simulation signal curves of excitation signals in modal test for the plane bidirectional tensile membrane structure. (**a**) Sweep excitation signal. (**b**) Transient excitation signal.

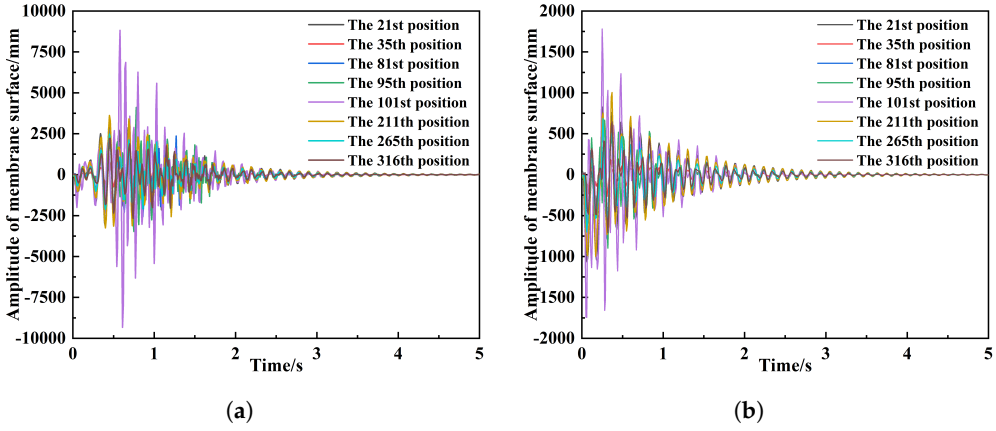


Figure 23. Curves of displacement vs time of sensor measuring locations under sweep excitation and transient excitation signals. (**a**) Sweep excitation signal. (**b**) Transient excitation signal.

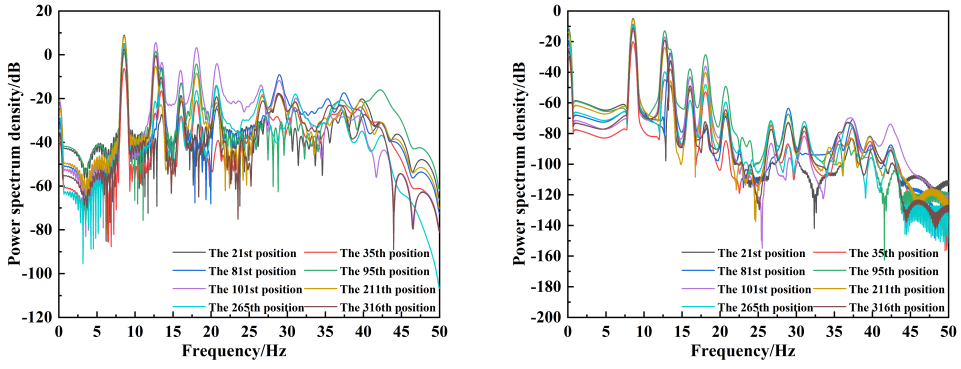


Figure 24. Curves of power spectrum density of sensor measuring locations under excitation signals. (**a**) Sweep excitation signal. (**b**) Transient excitation signal.

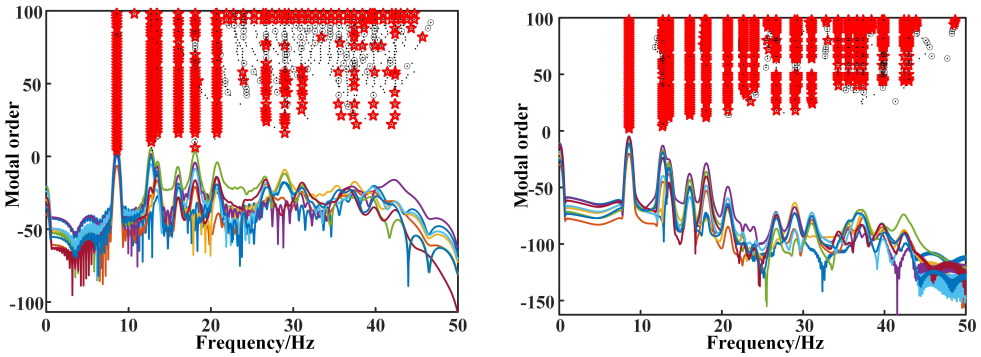


Figure 25. Comparison of modal parameter identification based on covariance stochastic subspace identification method under excitation signals. (**a**) Sweep excitation signal. (**b**) Transient excitation signal.

It can be found that IRSDPSO can almost accurately identify most modal frequencies within the first 19 modes of the tensile membrane structure through comparing the natural modal frequency with the identified frequency of the sweep excitation signal and the transient excitation signal as shown in Table 7 and Figure 26. In Figure 26, the red bar chart in Figure 26 represents the absolute value of the error between the natural frequency of the finite element simulation of the planar tensile membrane structure and the identified modal parameters in the vibration signal of the planar tensile membrane structure collected based on IRSDPSO layout measurement points. Although there is some error in high-order dense modal frequency identification of the tensile membrane structure, the identification error between the two can still be kept within 5%. Furthermore, by comparing the modal parameter identification of the two kinds of excitation signals, it can be found that the sweep excitation signal method can identify the dense modal frequency more accurately than the transient excitation signal for the high-order modal frequency. To sum up, it shows that the optimal placement of sensor measuring points based on the IRSDPSO proposed in this paper is reasonable and suitable, the validity and feasibility of which are verified by all results. The case of modal parameter identification also verifies that the IRSDPSO method can meet the requirements of using fewer sensors to predict unknown modal parameter information of the tensile membrane structures.

Table 7. Comparison of the first 35 ranks among simulation structural natural modal frequencies and the identified modal frequencies.

Modal Order	1	2	3	4	5	6	7
Frequency	8.58	12.73	12.73	13.46	16.03	18.04	18.04
Sweep identification	8.58	12.66	12.73	13.46	16.05	18.09	18.11
Transient identification	8.58	12.73	12.75	13.47	16.05	17.88	18.09
Modal order	8	9	10	11	12	13	14
Frequency	20.68	22.29	22.62	23.93	23.93	25.47	26.66
Sweep identification	20.61	21.88	22.74	22.93	23.93	25.26	26.36
Transient identification	20.73	22.65	22.67	23.98	NaN	25.65	26.62
Modal order	15	16	17	18	19	20	21
Frequency	26.66	28.93	29.16	29.27	31.03	31.03	33.18
Sweep identification	26.69	28.96	29.44	30.31	31.04	31.83	33.66
Transient identification	26.69	28.97	29.28	30.57	31.04	NaN	32.82
Modal order	22	23	24	25	26	27	28
Frequency	34.30	34.30	35.55	36.29	36.60	36.60	37.38
Sweep identification	34.59	NaN	35.55	NaN	36.59	NaN	37.38
Transient identification	34.28	NaN	35.56	NaN	36.63	NaN	37.39
Modal order	29	30	31	32	33	34	35
Frequency	39.72	39.85	39.92	39.92	41.88	42.40	42.98
Sweep identification	39.33	39.62	39.89	40.92	41.98	42.45	43.05
Transient identification	39.71	39.86	39.96	NaN	NaN	42.41	42.99

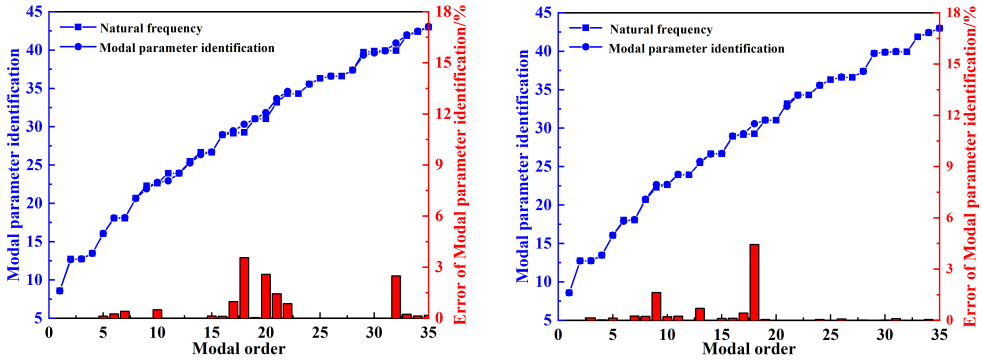


Figure 26. Comparison curves of structural natural modal frequencies and the identified modal frequencies. (**a**) Sweep excitation signal. (**b**) Transient excitation signal.

6. Conclusions

In order to optimize the OSP of health monitoring system in tensile membrane structures and meet the requirements of structural modal test parameter identification, this paper proposes an OSP method based on FIM and IRSDPSO. Two kinds of typical tensile membrane structure are modeled for studying the natural structural vibration characteristics, and the numerical modal test verification is carried out. The main results can be concluded as follows:

1. The modal order of the OSP for the tensile membrane structures is determined by using two-norm difference and trace change rate of FIM, and QR decomposition method and MAC criterion are used to select the number of sensors. After experiments, it

is determined that the modal order of the OSP for the plane bidirectional tensile membrane structure is the first five ranks, and the sensor arrangement conditions of sensors are eight, ten and twelve. Similarly, the modal order of the OSP for the umbrella-shaped membrane structure is the first twelve ranks, and the sensor arrangement conditions of sensors are fifteen, eighteen and twenty.

2. The sensor location optimization of tensile membrane structure is the discrete model that the traditional PSO algorithm cannot solve. For this reason, a new method of sensor location optimization based on IRSDPSO is proposed by improving the algorithm architecture, which uses mean square values of MAC off-diagonal elements to construct the fitness function for realizing sensor location optimization of two typical tensile membrane structures. The results show that IRSDPSO has good convergence and robustness. The effectiveness of IRSDPSO-based sensor location optimization is obviously superior to that using RDPSO.
3. The modal parameter identification of the plane bidirectional tensile membrane structure is simulated by means of sweep excitation and transient excitation analysis in ABAQUS steady-state dynamics. The covariance stochastic subspace identification method based on the time-domain identification method is applied to identify the modal parameters of the tensile membrane structure. The results show that the optimal sensor placement method based on FIM and IRSDPSO can not only accurately identify the first eleven modal parameters of the tensile membrane structures but also identify the higher-order modal parameters. This also indicates that IRSDPSO is reasonable and feasible in OSP for tensile membrane structures. The IRSDPSO method can predict unknown membrane structure modal parameter information with fewer sensors, and meet the demands of practical engineering health monitoring.
4. The optimal sensor placement results obtained in this paper are mainly applicable to modal monitoring objectives dominated by the Z-direction. In future work, the three-directional modal energy ratio, local normal response projection, or response fusion of triaxial sensors may be further introduced to improve the identification capability for high-order coupled modes, which will be interpreted as a complete coverage of the three-dimensional coupled dynamic response of the structure. It is worth noting that although the IRSDPSO algorithm has stable and efficient performance in the two tensile membrane structure cases used in this paper, further research is needed to investigate the OSP effect of the large-span tensile membrane structure with tens of thousands of nodes.

Author Contributions: Conceptualization, methodology, software, validation, investigation, formal analysis, Q.Y.; validation, X.Z.; data curation, Z.J. and C.P.; writing—original draft preparation, Q.Y.; writing—review and editing, X.Z.; project funding acquisition, Q.Y. All authors have read and agreed to the published version of the manuscript.

Funding: The authors are grateful for the financial support from the Fundamental Research Funds for the Central Universities (No. 2025QN1161,2025QN1068) and China Postdoctoral Science Foundation (No. 2025M771814).

Data Availability Statement: The original contributions presented in this study are included in the article. Further inquiries can be directed to the corresponding author.

Conflicts of Interest: The authors declare no conflicts of interest.

References

1. Sheng, L.; Zhang, Y.; Xu, J.; Li, X.; Zhao, Y. Tearing behavior of PVC-coated fabric with double initial cracks. *Thin Walled Struct.* **2025**, *211*, 113103. [CrossRef]
2. Hu, J.; Kawaguchi, K.; Ma, J. Long-term building thermal performance of enclosed large-span swimming stadiums with retractable membrane ceilings. *Energy Build.* **2020**, *207*, 109363. [CrossRef]
3. Shi, Q.; Wang, X.; Chen, W.; Hu, K. Optimal sensor placement method considering the importance of structural performance degradation for the allowable loadings for damage identification. *Appl. Math. Model.* **2020**, *86*, 384–403. [CrossRef]
4. An, H.; Youn, B.; Kim, H. A methodology for sensor number and placement optimization for vibration-based damage detection of composite structures under model uncertainty. *Compos. Struct.* **2022**, *279*, 114863. [CrossRef]
5. Craenenbroeck, M.; Puystiens, S.; Laet, L. Integrated analysis of kinematic form active structures for architectural applications: Experimental verification. *Eng. Struct.* **2016**, *123*, 59–70. [CrossRef]
6. Hassani, S.; Dackermann, U. A Systematic Review of Optimization Algorithms for Structural Health Monitoring and Optimal Sensor Placement. *Sensors* **2023**, *23*, 3293. [CrossRef] [PubMed]
7. Wang, W. Integrating data-driven reduced order models with Kriging for efficient sensor placement and full-field prediction. *Mech. Syst. Signal Process.* **2025**, *234*, 112760. [CrossRef]
8. Mazhar, M.; Hongki, J. Multi-objective sensor placement optimization for structural response estimation under spatially varying dynamic loading of bridges. *Adv. Struct. Eng.* **2021**, *24*, 2255–2266. [CrossRef]
9. Li, B.; Li, D.; Zhao, X.; Ou, J. Optimal sensor placement in health monitoring of suspension bridge. *Sci. China Technol. Sci.* **2012**, *55*, 2039–2047. [CrossRef]
10. Chang, M.; Pakzad, S. Optimal sensor placement for modal identification of bridge systems considering number of sensing nodes. *J. Bridge Eng.* **2014**, *19*, 040140191. [CrossRef]
11. An, J.; Kim, S.; Eun, H. Optimized sensor layout and monte carlo–based dMSE damage detection in truss structures using modal expansion. *Struct. Control. Health Monit.* **2026**, *2025*, 8645553. [CrossRef]
12. Haque, M. Adaptive multi-scale variational mode decomposition with transfer entropy for real-time detection of arrhythmia transitions in wearable ECG devices. In Proceedings of the 2026 5th International Conference on Electrical, Computer & Telecommunication Engineering (ICECTE), Rajshahi, Bangladesh, 29–31 January 2026. [CrossRef]
13. Argentino, A.; Bono, F.; Bernardini, L.; Romano, N.; Cazzulani, G.; Somaschini, C.; Belloli, M.; Cinquemani, S. Automated OMA through SSI-COV algorithm of a warren truss railway bridge exploiting free decay response. In Proceedings of the 10th International Operational Modal Analysis Confernece (IOMAC), Naples, Italy, 21–24 May 2024; pp. 600–608. [CrossRef]
14. Shi, Z.; Law, S.; Zhang, L. damage localization by directly using incomplete mode shapes. *J. Eng. Mech.* **2000**, *126*, 656–660. [CrossRef]
15. Guyan, R. Reduction of Stiffness and Mass Matrices. *AIAA J.* **1974**, *44*, 380–394. [CrossRef]
16. Reinbacher-Köstinger, A.; Gschwentner, A.; Mušeljić, E.; Kaltenbacher, M. Optimization of Sensor Placement for a Measurement System for the Determination of Local Magnetic Material Properties. *Mathematics* **2024**, *12*, 2220. [CrossRef]
17. Ponti, A.; Candelieri, A.; Giordani, I.; Archetti, F. Intrusion Detection in Networks by Wasserstein Enabled Many-Objective Evolutionary Algorithms. *Mathematics* **2023**, *11*, 2342. [CrossRef]
18. Nieminen, V.; Sopanen, J. Optimal sensor placement of triaxial accelerometers for modal expansion. *Mech. Syst. Signal Process.* **2023**, *184*, 109581. [CrossRef]
19. Kim, T.; Youn, B.; Oh, H. Development of a stochastic effective independence (SEFI) method for optimal sensor placement under uncertainty. *Mech. Syst. Signal Process.* **2018**, *111*, 615–627. [CrossRef]
20. Yi, T.; Li, H. Methodology Developments in Sensor Placement for Health Monitoring of Civil Infrastructures. *Int. J. Distrib. Sens. Netw.* **2014**, *8*, 612726. [CrossRef]
21. Yin, H.; Dong, K.; Pan, A.; Peng, Z.; Jiang, Z.; Li, S. Optimal sensor placement based on relaxation sequential algorithm. *Neurocomputing* **2019**, *344*, 28–36. [CrossRef]
22. Gomes, G.F.; da Cunha, S.S., Jr.; Alexandrino, P.d.L.; de Sousa, B.S.; Ancelotti, A.C., Jr. Sensor placement optimization applied to laminated composite plates under vibration. *Struct. Multidiscip. Optim.* **2018**, *58*, 2099–2118. [CrossRef]
23. Ni, Z.; Wu, S.; Wu, C. Time-varying frequency parameter identification of space solar power satellites based on an improved recursive subspace algorithm and optimal sensor placement. *Aerosp. Sci. Technol.* **2022**, *128*, 107754. [CrossRef]
24. Gomes, G.F.; de Almeida, F.A.; Alexandrino, P.d.L.; da Cunha, S.S., Jr.; de Sousa, B.S.; Ancelotti, A.C., Jr. A multiobjective sensor placement optimization for SHM systems considering Fisher information matrix and mode shape interpolation. *Eng. Comput.* **2019**, *35*, 519–535. [CrossRef]
25. Zhang, Z. Optimal layout of health monitoring sensor in gymnasium based on improved particle swarm optimization algorithm. *J. Intell. Fuzzy Syst.* **2018**, *35*, 2813–2819. [CrossRef]
26. Lin, C.; Zhang, C.; Chen, J. Optimal arrangement of structural sensors in soft rock tunnels based industrial IoT applications. *Comput. Commun.* **2020**, *156*, 159–167. [CrossRef]

27. Khalid, S.; Hwang, H.; Kim, H. Real-world data-driven machine-learning-based optimal sensor selection approach for equipment fault detection in a thermal power plant. *Mathematics* **2021**, *9*, 2814. [CrossRef]
28. El-Emam, M.; Zhou, L.; Yasser, E. Comparative analysis of numerical algorithms for modeling complex solid-liquid flow in a vertical conveying system with ceramic and expanded polystyrene particles. *Exp. Comput. Multiph. Flow* **2026**. [CrossRef]
29. Chen, Y.; Chen, W.; He, Y. Analysis and Test for the Space Different Thickness Film Structure in Still Air. In Proceedings of the International Conference on Structures and Building Materials (ICSBM 2013), Guizhou, China, 9–10 March 2013; pp. 611–617. [CrossRef]
30. Xu, J.; Zhang, Y.; Wu, M.; Li, X.; Zhang, L. Damping characteristics of the architectural coated fabric and its influence on the vibration response of membrane structures. *Compos. Struct.* **2022**, *285*, 115207. [CrossRef]
31. Sun, X.; Gong, D.; Zhou, K.; Zhou, J. Optimization of measurement points for vehicle body modal identification using particle swarm optimization. *Veh. Syst. Dyn.* 2026, *early access*. [CrossRef]

Disclaimer/Publisher's Note: The statements, opinions and data contained in all publications are solely those of the individual author(s) and contributor(s) and not of MDPI and/or the editor(s). MDPI and/or the editor(s) disclaim responsibility for any injury to people or property resulting from any ideas, methods, instructions or products referred to in the content.